JACS ARTICLES

Published on Web 03/12/2010

Effects of Dyes, Gold Nanocrystals, pH, and Metal Ions on Plasmonic and Molecular Resonance Coupling

Weihai Ni,[†] Huanjun Chen,[†] Jing Su,[‡] Zhenhua Sun,[†] Jianfang Wang,*[,†] and Hongkai Wu[‡]

Department of Physics, The Chinese University of Hong Kong, Shatin, NT, Hong Kong SAR, People's Republic of China, and Department of Chemistry, The Hong Kong University of Science and Technology, Clear Water Bay, Kowloon, Hong Kong SAR, People's Republic of China

Received December 3, 2009; E-mail: jfwang@phy.cuhk.edu.hk

Abstract: The effects of various factors on the resonance coupling between elongated Au nanocrystals and organic dyes have been systematically investigated through the preparation of hybrid nanostructures between Au nanocrystals and the electrostatically adsorbed dye molecules. A nanocrystal sample is chosen for each dye to match the longitudinal plasmon resonance wavelength with the absorption peak wavelength of the dye as close as possible so that the resonance coupling strength can be maximized. The resonance coupling strength is found to approximately increase as the molecular volume-normalized absorptivity is increased. It is mainly determined by the plasmon resonance energy of the Au nanocrystals instead of their shapes and sizes. Moreover, the resonance coupling can be reversibly controlled if the dye in the hybrid nanostructures is pH-sensitive. The coupling can also be weakened in the presence of metal ions. These results will be highly useful for designing resonance coupling-based sensing devices and for plasmon-enhanced spectroscopy.

Introduction

Interactions between noble metal nanocrystals and organic adsorbates can give rise to a variety of interesting phenomena, such as surface-enhanced Raman scattering, plasmon-enhanced fluorescence, enhancement of nonlinear optical signals, fluorescence quenching, energy transfer, and coupling between plasmonic and molecular resonances. Among them, plasmonic−molecular resonance coupling has attracted much attention from the perspectives of both fundamental understanding and practical applications. A large number of experimental[1−21] and theoretical[22–29] studies have been devoted to resonance coupling. Strong resonance coupling, which is usually revealed as a large plasmon peak splitting, occurs when the plasmonic resonance is degenerate with the molecular resonance. When the plasmon resonance energy is systematically varied across the molecular resonance energy, an anticrossing behavior is often observed. Many applications have been demonstrated with resonance coupling, including biological sensing[30,31] and imaging,[32,33] control of

[†] The Chinese University of Hong Kong.
[‡] The Hong Kong University of Science and Technology

(1) Wiederrecht, G. P.; Wurtz, G. A.; Bouhelier, A. *Chem. Phys. Lett.* **2008**, *461*, 171–179.
(2) Zhao, J.; Sherry, L. J.; Schatz, G. C.; Van Duyne, R. P. *IEEE J. Sel. Top. Quantum Electron.* **2008**, *14*, 1418–1429.
(3) Kometani, N.; Tsubonishi, M.; Fujita, T.; Asami, K.; Yonezawa, Y. *Langmuir* **2001**, *17*, 578–580.
(4) Wiederrecht, G. P.; Wurtz, G. A.; Hranisavljevic, J. *Nano Lett.* **2004**, *4*, 2121–2125.
(5) Bellessa, J.; Bonnand, C.; Plenet, J. C.; Mugnier, J. *Phys. Rev. Lett.* **2004**, *93*, 036404.
(6) Dintinger, J.; Klein, S.; Bustos, F.; Barnes, W. L.; Ebbesen, T. W. *Phys. Rev. B* **2005**, *71*, 035424.
(7) Haes, A. J.; Zou, S. L.; Zhao, J.; Schatz, G. C.; Van Duyne, R. P. *J. Am. Chem. Soc.* **2006**, *128*, 10905–10914.
(8) Bonnand, C.; Bellessa, J.; Plenet, J. C. *Phys. Rev. B* **2006**, *73*, 245330.
(9) Sugawara, Y.; Kelf, T. A.; Baumberg, J. J.; Abdelsalam, M. E.; Bartlett, P. N. *Phys. Rev. Lett.* **2006**, *97*, 266808.
(10) Zhao, J.; Jensen, L.; Sung, J. H.; Zou, S. L.; Schatz, G. C.; Van Duyne, R. P. *J. Am. Chem. Soc.* **2007**, *129*, 7647–7656.
(11) Uwada, T.; Toyota, R.; Masuhara, H.; Asahi, T. *J. Phys. Chem. C* **2007**, *111*, 1549–1552.
(12) Wurtz, G. A.; Evans, P. R.; Hendren, W.; Atkinson, R.; Dickson, W.; Pollard, R. J.; Zayats, A. V. *Nano Lett.* **2007**, *7*, 1297–1303.
(13) Ni, W. H.; Yang, Z.; Chen, H. J.; Li, L.; Wang, J. F. *J. Am. Chem. Soc.* **2008**, *130*, 6692–6693.
(14) Fofang, N. T.; Park, T.-H.; Neumann, O.; Mirin, N. A.; Nordlander, P.; Halas, N. J. *Nano Lett.* **2008**, *8*, 3481–3487.
(15) Nishi, H.; Asahi, T.; Kobatake, S. *J. Phys. Chem. C* **2009**, *113*, 17359–17366.
(16) Juluri, B. K.; Lu, M. Q.; Zheng, Y. B.; Huang, T. J.; Jensen, L. *J. Phys. Chem. C* **2009**, *113*, 18499–18503.
(17) Yoshida, A.; Yonezawa, Y.; Kometani, N. *Langmuir* **2009**, *25*, 6683–6689.
(18) Yoshida, A.; Uchida, N.; Kometani, N. *Langmuir* **2009**, *25*, 11802–11807.
(19) Cade, N. I.; Ritman-Meer, T.; Richards, D. *Phys. Rev. B* **2009**, *79*, 241404.
(20) Bellessa, J.; Symonds, C.; Vynck, K.; Lemaitre, A.; Brioude, A.; Beaur, L.; Plenet, J. C.; Viste, P.; Felbacq, D.; Cambril, E.; Valvin, P. *Phys. Rev. B* **2009**, *80*, 033303.
(21) Hakala, T. K.; Toppari, J. J.; Kuzyk, A.; Pettersson, M.; Tikkanen, H.; Kunttu, H.; Törmä, P. *Phys. Rev. Lett.* **2009**, *103*, 053602.
(22) Ambjörnsson, T.; Mukhopadhyay, G. *J. Phys. A: Math. Gen.* **2003**, *36*, 10651–10665.
(23) Ambjörnsson, T.; Apell, S. P.; Mukhopadhyay, G. *Phys. Rev. E* **2004**, *69*, 031914.
(24) Ambjörnsson, T.; Mukhopadhyay, G.; Apell, S. P.; Käll, M. *Phys. Rev. B* **2006**, *73*, 085412.
(25) Zhang, W.; Govorov, A. O.; Bryant, G. W. *Phys. Rev. Lett.* **2006**, *97*, 146804.
(26) Neuhauser, D.; Lopata, K. *J. Chem. Phys.* **2007**, *127*, 154715.
(27) Kelley, A. M. *Nano Lett.* **2007**, *7*, 3235–3240.
(28) Trügler, A.; Hohenester, U. *Phys. Rev. B* **2008**, *77*, 115403.

 10.1021/ja910239b

molecular energy redistribution,[34] infrared detection,[35] and molecular switches.[36] Moreover, understanding the resonance coupling is also important for plasmon-enhanced spectroscopy. For example, in surface-enhanced Raman scattering, the enhancement factor has been found to be largest when the plasmon wavelength is between the Raman excitation and emission energies.[37,38]

A number of different Ag and Au nanostructures have been employed in the previous experimental studies of resonance coupling. They include thin films,[5,8,19,21] nanovoids,[9] hole arrays,[6] nanodisk arrays,[7,10,20] spherical nanoparticles,[3,4,11,15,17] nanoshells,[14] nanorods,[13,16,18] and nanorod assemblies.[12] The plasmon resonance energies of some of these nanostructures can be varied over a wide range by control of their dimensions. In most of these previous experiments, only one dye per study was utilized. The dependence of the resonance coupling on the molecular properties of dyes has therefore remained unexplored. Here we report on a systematic investigation of how the resonance coupling is dependent on the molecular properties of dyes and the plasmonic properties of metal nanocrystals as well as external stimuli, including pH and metal ions. Elongated Au nanocrystals with varying longitudinal plasmon resonance wavelengths (LPRWs) and a variety of organic dyes were employed to construct nanocrystal−dye hybrid nanostructures through electrostatic attractive interaction. For each dye, a nanocrystal sample was made to have its LPRW as close as possible to the absorption peak wavelength of the dye so that a maximum resonance coupling strength could be obtained. The plasmon shift induced by the coupling between the longitudinal plasmon and the molecular absorption was determined as a function of the dye concentration, the nanocrystal shape and size, the solution pH, and the concentration of added metal ions.

Experimental Section

Preparation of Gold Nanorods with Different LPRWs. Five Au nanorod samples with decreasing LPRWs were prepared. The longest one, having an ensemble peak LPRW of 740 nm, was grown in aqueous solutions using a one-step seed-mediated method.[39] Specifically, the seed solution was made by the addition of $HAuCl_4$ (0.25 mL, 0.01 M) into cetyltrimethylammonium bromide (CTAB, 9.75 mL, 0.1 M) in a plastic tube. After the solution was mixed by inversion, a freshly prepared, ice-cold $NaBH_4$ solution (0.6 mL, 0.01 M) was added all at once, followed by rapid inversion mixing for 2 min. The resultant CTAB-stabilized Au nanoparticle seed solution was kept at room temperature for 2−4 h before use. The growth solution was made by mixing $HAuCl_4$ (2 mL, 0.01 M) and $AgNO_3$ (0.4 mL, 0.01 M) with CTAB (40 mL, 0.1 M) in a plastic tube. HCl (0.8 mL, 1.0 M) was then added, followed by the addition of a freshly prepared ascorbic acid solution (0.32 mL, 0.1 M). The resultant solution was mixed and then the seed solution (0.02 mL) was added. The reaction mixture was agitated by gentle inversion for 10 s and left undisturbed at least overnight.

The other four nanorod samples were prepared by oxidation shortening.[40] The nanorod sample with a LPRW of 740 nm was employed as the starting one, and H_2O_2 (35 wt %) was used as the oxidation agent. The volume ratio between the H_2O_2 solution and the as-grown nanorod solution was adjusted to 1:20. At this volume ratio, the longitudinal plasmon peak of the nanorod sample blue-shifted at a rate of ∼2 nm per min. The oxidation reaction was arrested at controlled periods of time by centrifugation and redispersion into water. The oxidation process gave the other four nanorod samples with LPRWs of 687, 658, 620, and 582 nm, respectively.

Preparation of Gold Nanocrystals with Different Shapes and Sizes but the Same LPRW. Seven elongated Au nanocrystal samples with different shapes and sizes were prepared. Their LPRWs were all around 735 nm. For ease of description, they are named thin nanorods, fat nanorods, dog-bone-like nanorods, small nanorods, large nanorods, small nanobipyramids, and large nanobipyramids, respectively. The seven nanocrystal samples were prepared in aqueous solutions by using the seed-mediated method together with oxidation shortening and transverse overgrowth.[41,42] Specifically, the growth of the fat nanorods followed the same procedure as that described above for the growth of the nanorods with a LPRW of 740 nm.

The small nanorods were produced by shortening a starting nanorod sample with a LPRW of 955 nm. For the growth of the starting nanorod sample, the seed solution was prepared by the addition of $NaBH_4$ (0.6 mL, 0.01 M) into a mixture composed of $HAuCl_4$ (0.25 mL, 0.01 M) and CTAB (9.75 mL, 0.1 M). The growth solution was made by the sequential addition of $HAuCl_4$ (2 mL, 0.01 M), $AgNO_3$ (0.6 mL, 0.01 M), HCl (0.8 mL, 1.0 M), and ascorbic acid (0.32 mL, 0.1 M) into CTAB (40 mL, 0.1 M). After the resultant solution was mixed by swirling for 30 s, 0.3 mL of the seed solution was added. The reaction solution was gently inversion-mixed for 2 min and then left undisturbed overnight. The obtained nanorods were subjected to oxidation shortening by adding HCl (0.2 mL, 1.0 M) in the as-grown nanorod solution (10 mL), followed by bubbling O_2 for 10 min. The plastic tube containing the solution was kept uncapped and transferred in an isothermal oven at 65 °C to initiate oxidation. The oxidation process was monitored spectrophotometrically. It was stopped by centrifugation and redispersion in water when the LPRW reached the desired value.

The thin nanorods were obtained by shortening a nanorod sample with a LPRW of 810 nm. The seed solution for this nanorod sample was prepared by the addition of $NaBH_4$ (0.3 mL, 0.01 M) into a mixture composed of $HAuCl_4$ (0.125 mL, 0.01 M) and CTAB (3.75 mL, 0.1 M). The growth solution was made by the sequential addition of $HAuCl_4$ (1.8 mL, 0.01 M), $AgNO_3$ (0.27 mL, 0.01 M), and ascorbic acid (0.288 mL, 0.1 M) into CTAB (42.75 mL, 0.1 M). Then 0.25 mL of the seed solution was added. The obtained nanorods were subjected to shortening to give the thin nanorods.

The preparation of the dog-bone-like nanorods was similar to that of the nanorods with a LPRW of 810 nm, except that the amount of the seed solution was changed from 0.25 to 0.15 mL.

The large nanorods were produced by transverse overgrowth on a pregrown nanorod sample with a LPRW of 887 nm. The preparation of the pregrown nanorod sample was similar to that of

(29) Yan, J.-Y.; Zhang, W.; Duan, S. Q.; Zhao, X.-G.; Govorov, A. O. *Phys. Rev. B* **2008**, *77*, 165301.
(30) Zhao, J.; Das, A.; Zhang, X. Y.; Schatz, G. C.; Sligar, S. G.; Van Duyne, R. P. *J. Am. Chem. Soc.* **2006**, *128*, 11004–11005.
(31) Zhao, J.; Das, A.; Schatz, G. C.; Sligar, S. G.; Van Duyne, R. P. *J. Phys. Chem. C* **2008**, *112*, 13084–13088.
(32) Liu, G. L.; Long, Y.-T.; Choi, Y.; Kang, T.; Lee, L. P. *Nat. Methods* **2007**, *4*, 1015–1017.
(33) Choi, Y.; Kang, T.; Lee, L. P. *Nano Lett.* **2009**, *9*, 85–90.
(34) Wiederrecht, G. P.; Hall, J. E.; Bouhelier, A. *Phys. Rev. Lett.* **2007**, *98*, 083001.
(35) Neubrech, F.; Pucci, A.; Cornelius, T. W.; Karim, S.; García-Etxarri, A.; Aizpurua, J. *Phys. Rev. Lett.* **2008**, *101*, 157403.
(36) Zheng, Y. B.; Yang, Y.-W.; Jensen, L.; Fang, L.; Juluri, B. K.; Flood, A. H.; Weiss, P. S.; Stoddart, J. F.; Huang, T. J. *Nano Lett.* **2009**, *9*, 819–825.
(37) Willets, K. A.; Van Duyne, R. P. *Annu. Rev. Phys. Chem.* **2007**, *58*, 267–297.
(38) Camden, J. P.; Dieringer, J. A.; Zhao, J.; Van Duyne, R. P. *Acc. Chem. Res.* **2008**, *41*, 1653–1661.
(39) Sau, T. K.; Murphy, C. J. *Langmuir* **2004**, *20*, 6414–6420.
(40) Tsung, C.-K.; Kou, X. S.; Shi, Q. H.; Zhang, J. P.; Yeung, M. H.; Wang, J. F.; Stucky, G. D. *J. Am. Chem. Soc.* **2006**, *128*, 5352–5353.
(41) Kou, X. S.; Zhang, S. Z.; Yang, Z.; Tsung, C.-K.; Stucky, G. D.; Sun, L. D.; Wang, J. F.; Yan, C. H. *J. Am. Chem. Soc.* **2007**, *129*, 6402–6404.
(42) Ni, W. H.; Kou, X. S.; Yang, Z.; Wang, J. F. *ACS Nano* **2008**, *2*, 677–686.

the nanorods with a LPRW of 740 nm, except that the amount of the seed solution was changed from 0.02 to 0.096 mL. The overgrowth solution was prepared by mixing together CTAB (152 mL, 0.1 M), $HAuCl_4$ (6.4 mL, 0.01 M), $AgNO_3$ (0.96 mL, 0.01 M), and ascorbic acid (1.024 mL, 0.1 M). Glutathione, which bonds preferentially to the ends of CTAB-stabilized Au nanorods[43] and thus induces transverse overgrowth, was added into the pregrown nanorod solution to reach a concentration of 0.1 mM. After 2 h, 2.0 mL of the pregrown nanorod solution was then placed into a plastic tube, followed by the addition of the overgrowth solution (4.5 mL). The growth was left undisturbed for more than 10 h.

The small Au nanobipyramids were grown using the seed-mediated method with citrate-stabilized Au nanoparticles as seeds.[44,45] The seed solution was made by adding $NaBH_4$ (0.15 mL, 0.01 M) under vigorous stirring into a mixture composed of $HAuCl_4$ (0.125 mL, 0.01 M), sodium citrate (0.25 mL, 0.01 M), and water (9.625 mL). The resultant citrate-stabilized seed solution was kept at room temperature for 2 h before use. The growth solution was made by the sequential addition of $HAuCl_4$ (1.2 mL, 0.01 M), $AgNO_3$ (0.06 mL, 0.01 M), and ascorbic acid (0.402 mL, 0.1 M) into cetyltributylammonium bromide (28.5 mL, 0.01 M). Then 0.45 mL of the seed solution was added to the growth solution, followed by gentle inversion mixing for 10 s. The resultant solution was left undisturbed overnight in an isothermal oven at 65 °C. The obtained small nanobipyramids have a LPRW of 729 nm. The large nanobipyramids were produced by oxidation shortening of a nanobipyramid sample with a LPRW of 886 nm. The growth of the starting nanobipyramid sample was carried out by changing the citrate-stabilized seed solution from 0.45 to 0.20 mL.

Preparation of Gold Nanocrystal−Dye Hybrid Nanostructures. The hybrid nanostructures were prepared through electrostatic attractive interactions. The as-prepared Au nanocrystals are positively charged owing to the encapsulation of the cationic surfactants. They were first turned to be negatively charged by adsorption of a layer of negatively charged polyelectrolyte, poly(sodium 4-styrenesulfonate) (PSS, MW 70 000).[46] Specifically, 20 mL of each Au nanocrystal sample was centrifuged at 6300*g* for 15 min to remove the excess surfactant in the solution. The precipitate was redispersed in water (10 mL) and subsequently added dropwise to an aqueous PSS solution (10 mL, 2 g/L, 6 mM NaCl) under vigorous stirring. After the solution was stirred for 3 h, the excess PSS was removed by centrifugation, and the resultant PSS-coated Au nanocrystals were redispersed in water (20 mL). Eight dyes, rhodamine 640, cresyl violet 670, malachite green, oxazine 720, oxazine 725, methylene blue, DOTCI, and HITC, were used for the preparation of Au nanocrystal−dye hybrid nanostructures. The aqueous stock solutions of the eight dyes were first prepared. Their concentrations were 92, 83, 216, 67, 100, 100, 18, and 68 μM, respectively. Each hybrid nanostructure solution was made by mixing the PSS-coated Au nanocrystal solution (0.05 mL) and the stock dye solution (0.02−0.95 mL) in a small plastic tube. The volume of the nanostructure solution was adjusted to 1 mL by adding an appropriate volume of water. The resultant mixture solution was kept undisturbed for more than 30 min before extinction spectral measurements.

The pH effect on the resonance coupling was investigated on a nanorod−HITC hybrid nanostructure sample, which was prepared by mixing the PSS-coated nanorod solution (0.5 mL), the stock HITC solution (1 mL, 68 μM), and water (8.5 mL). The mixture solution was kept undisturbed for more than 30 min before further treatments. The pH of the hybrid nanostructure solution was adjusted alternately with aqueous NaOH (1 M) and HCl (1 M) solutions.

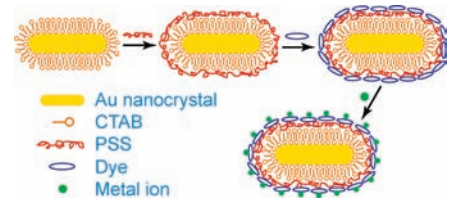

Figure 1. Schematic showing the sequential adsorption of the PSS chains, dye molecules, and metal ions onto the surfactant-stabilized Au nanorods.

The nanorod−dye hybrid nanostructure solutions used for the investigation of the effect of metal ions on the resonance coupling were made by mixing the PSS-coated nanorod solution (0.05 mL), the stock dye solution (0.05 mL), and water (0.9 mL). After the mixture solutions were kept undisturbed for more than 30 min, varying volumes of aqueous $Ni(NO_3)_2$ (10 mM), $CdCl_2$ (10 mM), $FeCl_2$ (10 mM), and $Hg(NO_3)_2$ (10 mM) solutions were added separately into the hybrid nanostructure solutions. The mixture solutions were kept undisturbed again for more than 30 min before extinction spectral measurements.

Calculation of Molecular Volumes. A software package, ChemBioOffice 2008, from CambridgeSoft was utilized to generate three-dimensional molecular structures and solvent-accessible surfaces of the eight dyes. The atom positions and bond angles of each dye molecule were optimized so that its total potential energy was minimized and a stable molecular structure was obtained. The three-dimensional solvent-accessible surface of each dye molecule was produced with H_2O as a probe molecule. The molecular volume enclosed by the three-dimensional surface was thereafter calculated.

Characterization Techniques. Extinction and absorption spectra were recorded on a Hitachi U-3501 UV/visible/NIR spectrophotometer. For the measurement of the absorption spectra of the dyes, the concentrations were adjusted to 10 μM for all of the dyes. Transmission electron microscopy (TEM) imaging was performed on an FEI CM120 microscope at 120 kV. A pH meter (pHTestr20) from Eutech Instruments was employed to measure the pH of the hybrid nanostructure solutions. Digital pictures were taken with a Nikon Coolpix 4500 camera.

Results and Discussion

Effect of the Molecular Properties of Dyes. The as-prepared Au nanocrystals are stabilized with the cationic surfactants and positively charged. Because a number of commercially available dyes are also positively charged, the nanocrystals were first wrapped with a PSS layer according to a modified layer-by-layer assembly method.[46] The PSS layer is negatively charged and therefore facilitates the adsorption of positively charged dye molecules to give the nanocrystal−dye hybrid nanostructures (Figure 1). Our previous TEM characterization showed that the spacing between the dye and the metal surface in such prepared hybrid nanostructures is 1.4 ± 0.2 nm.[13]

Five Au nanorod samples were prepared for the investigation of the effect of different dyes on the resonance coupling. These nanorods are cylindrical in the middle section and capped with a half sphere at each end (Figure 2). Noble metal nanorods typically exhibit two plasmon modes. One is the transverse mode, and the other is the longitudinal mode. They correspond to the electron oscillations perpendicular and parallel to the length axis, respectively. Because the longitudinal plasmon energy can be synthetically controlled by varying the nanorod length, the longitudinal plasmon of the nanorods was employed in our experiments. Anisotropic oxidation was carried out

(43) Kou, X. S.; Sun, Z. H.; Yang, Z.; Chen, H. J.; Wang, J. F. *Langmuir* **2009**, *25*, 1692–1698.
(44) Kou, X. S.; Zhang, S. Z.; Tsung, C.-K.; Yeung, M. H.; Shi, Q. H.; Stucky, G. D.; Sun, L. D.; Wang, J. F.; Yan, C. H. *J. Phys. Chem. B* **2006**, *110*, 16377–16383.
(45) Kou, X. S.; Ni, W. H.; Tsung, C.-K.; Chan, K.; Lin, H.-Q.; Stucky, G. D.; Wang, J. F. *Small* **2007**, *3*, 2103–2113.
(46) Pastoriza-Santos, I.; Pérez-Juste, J.; Liz-Marzán, L. M. *Chem. Mater.* **2006**, *18*, 2465–2467.

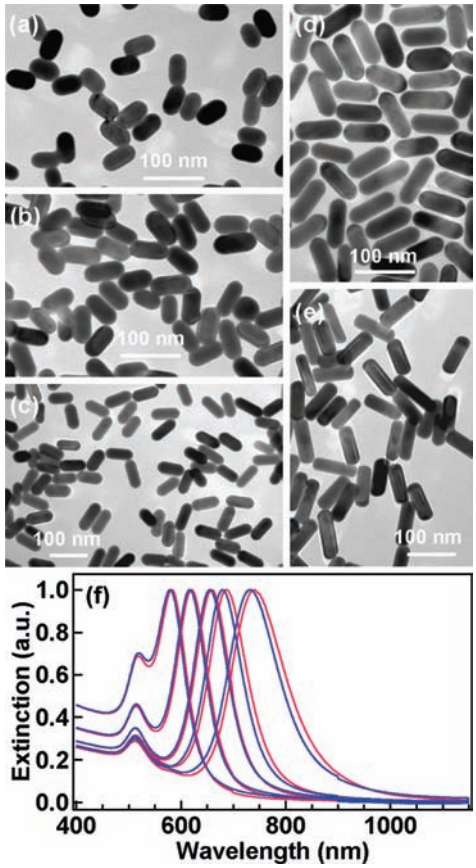

Figure 2. Gold nanorod samples with varying LPRWs. (a−e) TEM images of the nanorod samples with increasing LPRWs. (f) Normalized extinction spectra of the CTAB-stabilized nanorod samples (red) and the corresponding PSS-coated ones (blue).

Table 1. Average Diameters, Lengths, Aspect Ratios, and Ensemble LPRWs of the Five Gold Nanorod Samples

diameter[a] (nm)	length[a] (nm)	aspect ratio[a]	LPRW, CTAB stabilized (nm)	LPRW, PSS-coated (nm)
31 (2)	52 (4)	1.7 (0.1)	582	580
31 (2)	63 (5)	2.0 (0.2)	620	616
31 (2)	72 (5)	2.3(0.2)	658	655
31 (3)	80 (7)	2.6 (0.3)	687	680
30 (3)	91 (7)	3.0 (0.4)	740	732

[a] Numbers in parentheses are standard deviations.

carefully on the longest nanorods to obtain shorter nanorods.[40,42] The resultant nanorods have the same diameter at 31 nm but varying lengths from 90 to 50 nm (Table 1). As expected, their LPRWs decrease with decreasing lengths, ranging from 740 to 580 nm (Figure 2f). The longitudinal plasmon peaks of these nanorods exhibit slight blue shifts after the PSS coating (Figure 2f and Table 1).

Eight dyes were selected for our studies. They are rhodamine 640, cresyl violet 670, malachite green, oxazine 720, oxazine 725, methylene blue, DOTCI, and HITC. Figure 3 shows their molecular structures and absorption spectra. All of these dyes exhibit a major absorption peak together with a vibrational shoulder at the shorter-wavelength side. The peak wavelengths are in the range of 570−740 nm, and the peak absorption coefficients vary from 0.4×10^5 to 1.6×10^5 M^{-1} cm^{-1} (Table 2).

A plasmon peak will be split into two peaks when the plasmon resonance is coupled with the molecular resonance of

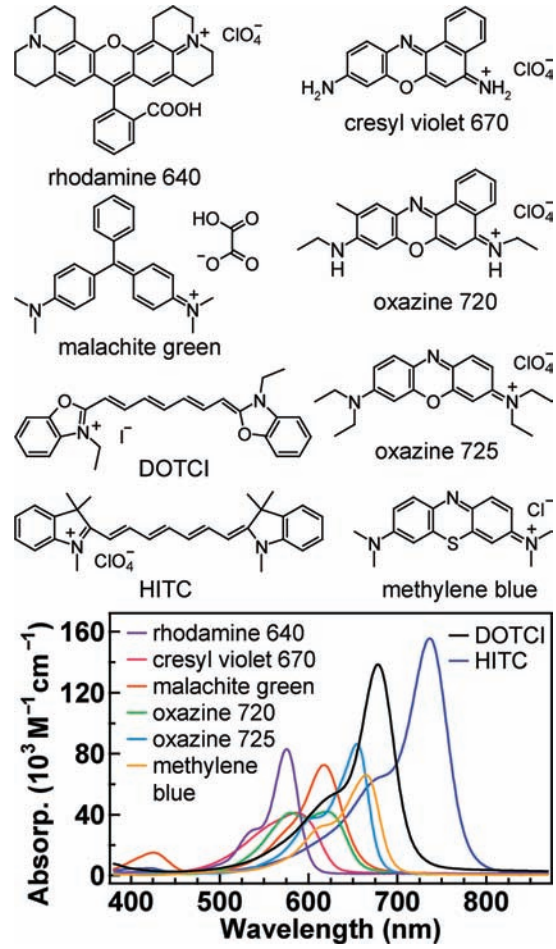

Figure 3. Molecular structures and absorption spectra of the eight dye molecules. The left axis is the absorptivity.

an ideal dye that has only one sharp absorption peak. As the plasmon energy is systematically varied across the molecular resonance energy by using noble metal nanostructures of different sizes, an anticrossing behavior is usually observed.[5,8,12–14,18,19,24] The coupling strength is highest when the plasmonic and molecular energies are degenerate. Because our goal is to study the effect of the molecular properties of dyes on the resonance coupling, the shortening of the Au nanorods through anisotropic oxidation was deliberately controlled so that the nanorod sample that had the LPRW as close as possible to the major absorption peak wavelength was produced for each dye. The actual LPRW of the PSS-coated nanorod sample used for each dye is listed in Table 2. The near degeneracy between the plasmonic and molecular resonance energies ensures that the resonance coupling behaviors of the different dyes can be compared and the intrinsic effect of their molecular properties on the resonance coupling can be ascertained.

The dyes are all positively charged. They can readily be adsorbed on the negatively charged PSS-coated Au nanorods through electrostatic interactions to form the nanorod−dye hybrid nanostructures. Because the coupling strength increases with increasing amounts of adsorbed dye molecules,[13,16,22–24] the nanorod concentration was kept fixed approximately in the range 0.1−0.3 nM, and the dye concentration was gradually increased in order to determine the maximum coupling strength. As an example, Figure 4a shows the extinction spectra recorded as a function of the dye concentration for rhodamine 640. The black curve is the extinction spectrum of the PSS-coated Au

Table 2. Molecular Properties and Langmuir Fitting Constants of the Eight Dyes

dye	absorption wavelength [a] (nm)	molecular volume (nm^3)	peak absorptivity[b] ($1000\ M^{-1}\ cm^{-1}$)	LPRW, PSS-coated (nm)	Langmuir equilibrium constant (μM^{-1})	maximum plasmon shift[c] (nm/cm^{-1})
rhodamine 640	575	1.34	83.1	580	4.00	45 (1)/1240 (50)
cresyl violet 670	586	0.54	41.3	580	0.14	58 (3)/1570 (150)
malachite green	617	1.09	72.6	616	3.13	46.5 (0.3)/1140 (10)
oxazine 720	620	0.74	42.0	616	1.59	52 (3)/1260 (130)
oxazine 725	654	1.03	86.4	655	0.82	53 (2)/1140 (80)
methylene blue	664	0.70	66.1	680	0.16	54 (6)/1080 (220)
DOTCI	678	1.03	138.5	680	0.36	117 (15)/2160 (470)
HITC	736	1.18	155.6	732	1.15	131 (7)/2070 (190)

[a] Wavelength of the major absorption peak. [b] Absorptivity of the major absorption peak. [c] Numbers in parentheses are standard deviations.

nanorods in the absence of rhodamine 640. With the addition of rhodamine 640 and gradual increase in its concentration, the plasmon peaks of the nanorods are overwhelmed by the absorption peaks of the dye. At the same time, a new peak at the longer-wavelength side of the major absorption peak evolves and becomes prominent. This new peak is ascribed to the lower-energy one of the two split longitudinal plasmon peaks arising from the strong resonance coupling.

Each extinction spectrum acquired at different concentrations of rhodamine 640 was fitted with multiple Lorentzian peaks (Figure S1 in the Supporting Information). When the strong resonance coupling occurs, the plasmon peak is usually split into two peaks, with one at the shorter-wavelength side and the other at the longer-wavelength side.[5,8,12–14,18,19,24] In our experiments, all of the dyes have a vibrational shoulder at the shorter-wavelength side of their major absorption peaks, and the transverse plasmon peak of the nanorods is also at the shorter-wavelength side. In addition, both the dyes and the nanorods exhibit increasing absorption toward the UV region. Moreover, the two split longitudinal plasmon peaks are broadened owing to the inhomogeneous size distribution of the Au nanorods. All of these factors make it difficult to determine the accurate wavelength of the higher-energy one of the two split longitudinal plasmon peaks by the curve fitting. However, because the lower-energy peak arising from the strong resonance coupling is the only one at the longer-wavelength side of the major absorption peak of the dye, its wavelength can be accurately determined by the curve fitting. The wavelength of the lower-energy peak was therefore obtained in our experiments for all of the Au nanocrystal−dye hybrid nanostructures. The plasmon shift, which is defined as the difference between the lower-energy peak wavelength of the hybrid nanostructure and the LPRW of the corresponding PSS-coated nanorod sample, was calculated to compare the resonance coupling strengths among the different hybrid nanostructures.

Figure 4b shows the dependence of the plasmon shift on the dye concentration for rhodamine 640. There exists a sharp transition around 2 μM for this dye. Below 2 μM, the plasmon shift rises rapidly. Above 2 μM, it increases slowly and becomes saturated at higher concentrations of rhodamine 640. The concentration dependence of the plasmon shift can be well fitted with the Langmuir adsorption equation:

$$\Gamma = \frac{\Gamma_{max} KC}{1 + KC} \quad (1)$$

where Γ, Γ_{max}, K, and C refer to the plasmon shift, the maximum plasmon shift, the Langmuir equilibrium binding constant, and the dye concentration, respectively. The obtained maximum plasmon shift and the Langmuir binding constant for rhodamine 640 are 45 nm and 4.00 μM^{-1}, respectively. The same experiment and data analysis were also carried out for the other dyes. The extinction spectra recorded as a function of the dye concentration are shown in Figures S2−S8 in the Supporting Information, and the concentration dependence of the plasmon shift is shown in Figure 4c−i for cresyl violet 670, malachite green, oxazine 720, oxazine 725, methylene blue, DOTCI, and HITC, respectively. In addition, we carried out control experiments, where Au nanocrystals with plasmon wavelengths of 530−550 nm were employed and the concentrations of the dyes were also varied. These experiments confirm that the red-shifted peaks arise from the resonance coupling instead of the aggregation of the dye molecules (Figures S9 and S10, Supporting Information). The maximum plasmon shifts and the Langmuir binding constants obtained from the curve fitting for all of the dyes are listed in Table 2. The maximum plasmon shift, which reflects the resonance coupling strength between the nanorods and dyes, is believed to result when the adsorbed dye amount reaches the upper limit set by the electrostatic interaction between the PSS layer and the dye molecules. The equilibrium binding constant indicates the adsorption strength of the dye molecules to the PSS layer on the Au nanorods. It is related to the sharpness of the transition from the rapidly increasing region to the plateau region on the curve of the plasmon shift versus the dye concentration. The sharper the transition, the larger the binding constant (Figure 4b−i). Both the plasmon shift and the binding constant vary significantly among the different dyes. The plasmon shift for HITC is largest at 131 nm, while that for rhodamine 640 is smallest at 45 nm. The largest plasmon shift is ~3 times the smallest one. In terms of energy, the plasmon shift for DOTCI is largest at 2160 cm^{-1}, while that for methylene blue is smallest at 1080 cm^{-1}. The largest plasmon shift is ~1.9 times the smallest one. The binding constant of rhodamine 640 is largest at 4 μM^{-1}, while that of cresyl violet 670 is smallest at 0.14 μM^{-1}. The difference amounts to ~30 times.

Both the molecular oscillator strength and the number of adsorbed dye molecules play important roles in the resonance coupling.[22–24] The former is proportional to the molecular absorptivity, and the latter is inversely proportional to the molecular volume if the total volume occupied by the adsorbed dye molecules is fixed. In our experiments, the dye adsorption occurs through the electrostatic attractive interaction between the PSS layer and the positively charged dye molecules. This adsorption process sets an upper limit for the total volume occupied by the adsorbed dye molecules. We therefore plotted the maximum plasmon shift in energy as a function of the peak molecular absorptivity divided by the molecular volume (Figure 4j). For the calculation of the molecular volume, the total potential energy of each molecule was first minimized, and the

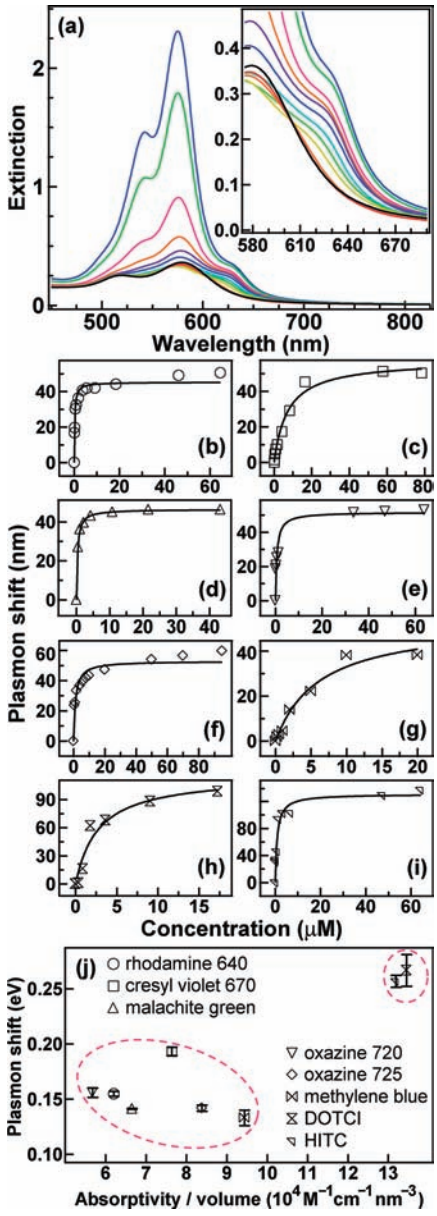

Figure 4. Resonance coupling between the Au nanorods and different dye molecules. (a) Extinction spectra of a PSS-coated nanorod sample in the presence of varying concentrations of rhodamine 640. The dye concentrations are 0, 0.1, 0.2, 0.5, 0.9, 1.8, 3.7, 5.5, 9.2, 18.4, 46.1, and 64.5 μM from bottom to top, respectively. The spectral region enlarged in the inset contains the low-energy split plasmon peak of the nanorods. (b−i) Plasmon shift as a function of the dye concentration for rhodamine 640, cresyl violet 670, malachite green, oxazine 720, oxazine 725, methylene blue, DOTCI, and HITC, respectively. The lines are fits according to the Langmuir equation. (j) Plasmon shift versus the peak molar absorptivity divided by the molecular volume. The data points are clustered into two regions, as indicated by the ellipses.

three-dimensional molecular surface was then mapped out using water as a probing molecule (Figure S11 in the Supporting Information). The volume enclosed by the molecular surface was taken as the molecular volume (Table 2). The data points for the eight dyes are seen to cluster into two regions in the plot. Those for rhodamine 640, cresyl violet 670, malachite green, oxazine 720, oxazine 725, and methylene blue are in the lower-left region, while those for DOTCI and HITC are in the upper-right region. Although the number of data points is limited by the availability of positively charged dyes, the plot suggests that the maximum plasmon shift and therefore the resonance coupling strength increase as the molecular volume-normalized absorptivity is increased.

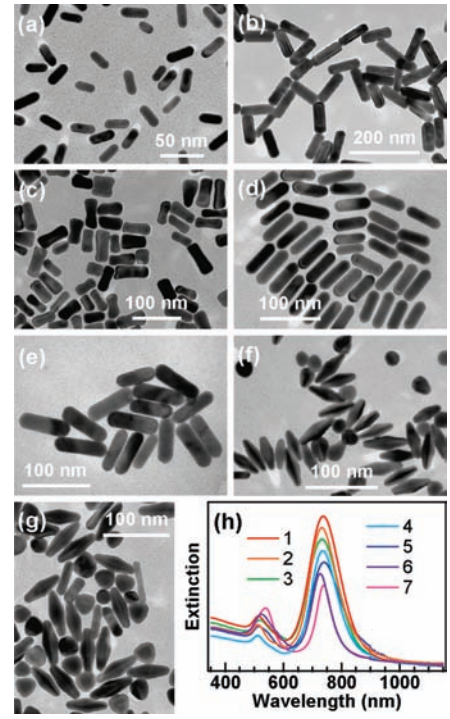

Figure 5. TEM images of the (a) thin nanorods, (b) fat nanorods, (c) dog-bone-like nanorods, (d) small nanorods, (e) large nanorods, (f) small nanobipyramids, and (g) large nanobipyramids. (h) Normalized extinction spectra of the PSS-coated Au nanocrystal samples. Curves 1−7 correspond to the samples shown in a−g, respectively.

Effect of the Shape and Size of Gold Nanocrystals with the Same LPRW. The plasmonic properties of noble metal nanocrystals are highly dependent on their shapes and sizes. Even if they possess the same plasmon wavelength, their absorption and scattering cross sections, local electric field enhancements, and refractive index sensitivities vary considerably among differently shaped and sized nanocrystals.[42,45,47] For example, electrodynamic calculations performed on a Au bipyramid and a Au nanorod that have the same LPRW at 775 nm show that the maximum electric field intensity enhancement of the bipyramid is ∼6 times that of the nanorods.[45] The refractive index sensitivities of variously shaped and sized Au nanocrystals that possess the same LPRW at 730 nm have been measured to range from 160−330 nm per refractive index unit.[47] We therefore prepared seven elongated Au nanocrystal samples with nearly the same LPRW but different shapes and sizes. Figure 5 shows the TEM images and extinction spectra of the seven nanocrystal samples. Their average diameters and lengths, measured from their respective TEM images, are given in Table 3. Four of the samples, including the thin, fat, small, and large nanorods, are cylindrical and have different diameters and lengths. One sample is dog-bone-like, with the ends thicker than the middle section. The other two samples are bipyramids, with two pentagonal pyramids base-to-base connected together.[44,45]

The LPRW of the seven Au nanocrystal samples is 735 nm. This wavelength is very close to the major absorption peak wavelength of HITC at 736 nm (Table 2). HITC was therefore chosen to make the hybrid nanostructures with these differently

(47) Chen, H. J.; Shao, L.; Woo, K. C.; Ming, T.; Lin, H.-Q.; Wang, J. F. *J. Phys. Chem. C* **2009**, *113*, 17691–17697.

Table 3. Average Diameters, Lengths, LPRWs, and Maximum Plasmon Shifts of the Seven Gold Nanocrystal Samples

gold nanocrystals	diameter[a] (nm)	length[a] (nm)	LPRW, PSS-coated (nm)	maximum plasmon shift (nm)
thin nanorods	10 (1)	26 (4)	736	159
fat nanorods	30 (3)	91 (7)	732	127
dog-bone-like nanorods	20 (2)	56 (5)	732	156
small nanorods	20 (1)	61 (5)	738	159
large nanorods	22 (2)	72 (10)	739	147
small nanobipyramids	19 (1)	55 (5)	727	142
large nanobipyramids	24 (1)	67 (4)	738	142

[a] Numbers in parentheses are standard deviations.

shaped nanocrystals so that the strong resonance coupling could be obtained. The preparation of the hybrid nanostructures followed the same procedure as described above. The concentration of HITC was controlled to be in the range of 20−50 μM to ensure that the resultant plasmon shift was in the saturated region on the Langmuir adsorption curve (Figure 4i). The effect of the dye concentration on the plasmon shift was therefore eliminated. The extinction spectra acquired before and after the addition of HITC are shown in Figure S12 in the Supporting Information for all seven Au nanocrystal samples. The plasmon shift values obtained from the curve fitting are listed in Table 3. They are very close to each other and average 147 ± 12 nm. The ratio between the standard deviation and the average value is 8%. This result indicates that the plasmon energy instead of the nanocrystal shape, size, and local electric field enhancement plays a major role in the resonance coupling between noble metal nanocrystals and molecular dyes.

Effect of pH. We have studied above the effects of the plasmonic properties of the Au nanocrystals and the molecular properties of the dyes on the resonance coupling. Such studies are important for understanding the fundamental aspects of the resonance coupling. On the other hand, exploring the response of the resonance coupling to external stimuli will have many technological applications. For example, the plasmon resonance of noble metal nanocrystals generally red-shifts as the refractive index of the surrounding nanoenvironment is increased. This effect is highly suitable for chemical and biological sensing, which has been demonstrated extensively.[37,48] However, the sensitivity is limited by the fact that the increase in the refractive index of the nanoenvironment is usually very small when biological molecules are bound to the surface of metal nanocrystals in aqueous solutions. New approaches are strongly needed for increasing the sensitivity. The resonance coupling provides an attractive sensing mechanism with potential for largely increasing the sensitivity, because the coupling-induced plasmon shift can reach 150 nm (Table 3) upon the adsorption of only one layer of organic molecules. We therefore carried out preliminary studies on how external stimuli, including pH and metal ions, can affect the resonance coupling. These experiments were performed with the commercially available dyes. For sensing, further efforts are required to design dyes that are optically active and can respond specifically to targeted analytes.

HITC possesses a major absorption peak at 736 nm. This absorption peak can be switched off nearly completely by adjusting the solution pH above 12. The switching is reversible. The absorption peak can be completely recovered by adjusting

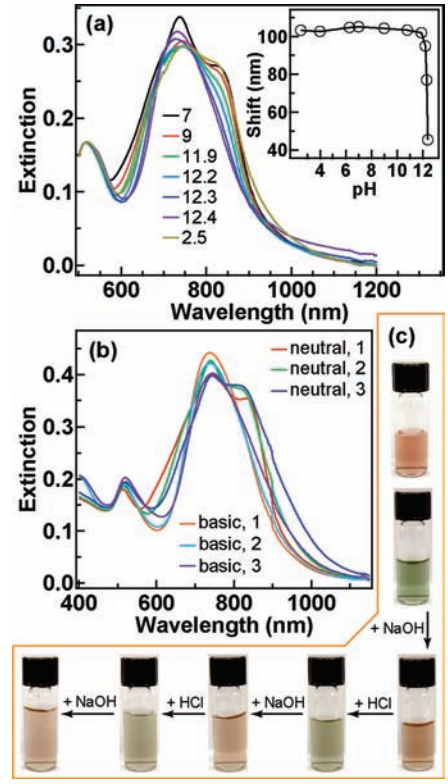

Figure 6. Effect of pH on the resonance coupling in the Au nanorod−HITC hybrid nanostructures. (a) Representative extinction spectra of the nanorod−HITC hybrid nanostructure solution acquired at varying pH values. The inset shows the dependence of the plasmon shift on the pH. (b) Extinction spectra showing three cycles of the resonance coupling and decoupling processes that are controlled by the pH. The basic and neutral conditions represent pH values of 12.3 and 7.0, respectively. (c) Digital pictures of the PSS-coated nanorod solution (right top) and the corresponding nanorod−HITC hybrid nanostructure solution during the coupling and decoupling processes.

the pH to ∼7 (Figure S13a in the Supporting Information). The reversible switching of the absorption can be ascribed to the breaking and restoration of the conjugated double bonds through the attachment and removal of a hydroxyl group to the carbon chain of HITC under high- and low-pH conditions, respectively (Figure S13b in the Supporting Information). The pH control of HITC adsorption allows us to investigate how the resonance coupling between the Au nanorods and HITC responds to the pH change. Figure 6a shows the representative extinction spectra of the Au nanorod−HITC hybrid nanostructure solution at varying pH values. The PSS-coated Au nanorod sample used in this experiment has a LPRW of 732 nm, which is very close to the major absorption peak wavelength of HITC. The concentration of HITC in the mixture solution is 6.8 μM. When the pH is below ∼12, a shoulder peak, which is the coupling-induced lower-energy peak, is clearly visible around 835 nm. When the pH is above ∼12, the shoulder peak is absent, suggesting the weakening of the resonance coupling. The inset in Figure 6a shows the extracted plasmon shift as a function of the pH. The plasmon shift is found to stay nearly constant below the pH of ∼12 and drop abruptly above the pH of ∼12. This dependence of the plasmon shift on the pH is ascribed to the switching off of HITC absorption at the high pH conditions.

The dependence of HITC absorption on the pH provides a means for reversibly controlling the resonance coupling strength between the Au nanorods and HITC. Figure 6b shows the extinction spectra of the hybrid nanostructure solution with its

(48) Anker, J. N.; Hall, W. P.; Lyandres, O.; Shah, N. C.; Zhao, J.; Van Duyne, R. P. *Nat. Mater.* **2008**, *7*, 442–453.

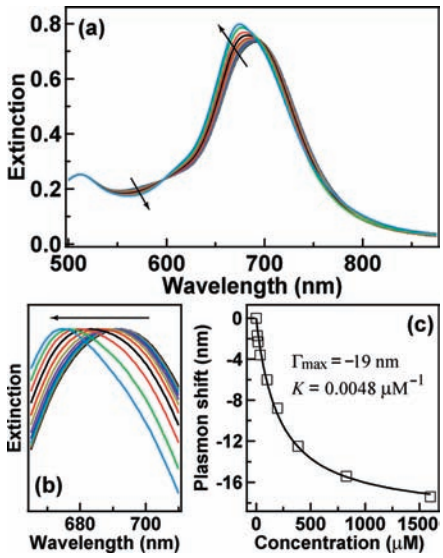

Figure 7. Effect of metal cations on the plasmonic and molecular resonance coupling. (a) Extinction spectra of the Au nanorod−methylene blue hybrid nanostructure solution acquired at varying concentrations of Ni^{2+}. The concentration of methylene blue in the original hybrid nanostructure solution is 5 μM. The concentrations of Ni^{2+} are 0, 8, 17, 35, 99, 196, 385, 826, and 1597 μM, respectively. The extinction spectra have been corrected for the dilution caused by the addition of Ni^{2+}. (b) Normalized extinction spectra shown in (a) in an enlarged view. (c) Plasmon shift versus the concentration of Ni^{2+}. The line is a fit according to the Langmuir equation.

pH controlled alternately to be low and high for three cycles. The resonance coupling is very strong when the pH is 7.0, while it becomes very weak when the pH is 12.3, as revealed by the appearance and disappearance of the shoulder peak. The reversible control of the resonance coupling is also accompanied with clear color changes (Figure 6c). The PSS-coated Au nanorod solution is originally red in color. It becomes green after the addition of HITC. This color change is induced by the strong resonance coupling. When the solution pH is adjusted to 12.3, the resonance coupling is nearly turned off, making the solution appear red again. This resonance coupling-induced color change is repeatable for many cycles.

Effect of Metal Ions. Methylene blue has previously been found to be able to bind to metal ions carrying two positive charges,[49,50] such as Ni^{2+}, Cd^{2+}, Fe^{2+}, and Hg^{2+}. These metal ions were therefore added in the mixture solution after the Au nanorod−methylene blue hybrid nanostructures were formed to investigate how these metal ions affect the resonance coupling (Figure 1). Figure 7a shows the representative extinction spectra recorded after the addition of varying concentrations of Ni^{2+}. The PSS-coated Au nanorod sample employed here has a LPRW of 680 nm. The concentration of the dye in the mixture solution is 5 μM. It was kept relatively low here so that a majority of the dye molecules could be adsorbed on the PSS-coated Au nanorods and that the effect of the metal ions was not disturbed by the adsorption of the dye. The original hybrid nanostructures give a coupling-induced lower-energy peak around 690 nm. This peak shows a blue shift upon the addition of Ni^{2+}. Both the magnitude of the blue shift and the peak intensity increase as more Ni^{2+} is added. At the same time, the extinction intensity around the wavelength of 570 nm decreases. The extinction intensity at this wavelength position can therefore be ascribed to the coupling-induced higher-energy peak. These spectral changes suggest that the resonance coupling is weakened. The resonance decoupling through the addition of metal ions also allows the coupling-induced higher-energy peak to be clearly identified, although it is hidden by many extinction contributions for the original nanorod−methylene blue hybrid nanostructures.

The extinction spectra acquired at varying Ni^{2+} concentrations were normalized against the resonance coupling-induced lower-energy peak maxima (Figure 7b). The blue shift of the peak is clearly visible on the normalized extinction spectra. The peak wavelengths were plotted as a function of the concentration of Ni^{2+} (Figure 7c). The plot can be well fitted with eq 1, the Langmuir adsorption equation. The resultant Γ_{max} and K are −19 nm and 0.0048 μM^{-1}, respectively. The maximum plasmon shift, Γ_{max}, is negative, because it is a blue shift. The experiment was also carried out with other metal ions and dyes. Cd^{2+}, Fe^{2+}, and Hg^{2+} were also found to be able to weaken the resonance coupling between the Au nanorods and methylene blue (Figure 14 in the Supporting Information). The maximum plasmon shifts obtained from the curve fitting are −18, −17, and −40 nm, and the equilibrium binding constants are 0.0089, 0.0025, and 0.034 μM^{-1}, respectively. The binding constants are very small, implying that the binding interaction between methylene blue molecules and the metal ions is very weak. The concentration of Hg^{2+} was kept below ~50 μM, because Hg^{2+} can react with the Au nanorods at higher concentrations. In addition, among the other seven dyes, only oxazine 725 was found to exhibit a response in terms of its resonance coupling with the Au nanorods (Figures S15 and S16 in the Supporting Information). These results suggest that the binding of the metal ions to methylene blue and oxazine 725 is probably due to the presence of a heterocycle containing a nitrogen and oxygen atom in their molecular structures (Figure 3). Cresyl violet 670 and oxazine 720 also contain such a heterocycle, but they have an additional benzene ring adjacent to the nitrogen atom. This additional benzene ring could act as a spatial barrier, which prevents the metal ions from binding to the nitrogen atom.

Control experiments were carried out to understand the effect of the metal ions on the resonance coupling (Figure S17 in the Supporting Information). First, the blue shift is not due to the dilution caused by the addition of the metal ion solutions. Second, the LPRW of the PSS-coated Au nanorods is not affected by the presence of the metal ions. Third, the absorption of methylene blue is not changed by the addition of the metal ions either. Fourth, the adsorbed dye molecules are not desorbed from the hybrid nanostructures after the addition of the metal ions. Although the absorption of methylene blue in aqueous solutions is not changed by the metal ions, we still believe that the metal ions can bind to the dye molecules that are adsorbed on the PSS-coated Au nanorods and change the absorption properties of the dye. Both the metal ions and the dye molecules are positively charged. The metal ions are therefore difficult to bind to the dye molecules in aqueous solutions. However, when the dye molecules are adsorbed on the PSS layer, their positive charges are neutralized or even overcompensated because the 4-styrenesulfonate monomer is smaller than the dye molecule. The charge neutralization allows the metal ions to bind to the dye molecules, change the absorption, and therefore weaken the resonance coupling. In addition, we also note that the maximum blue shifts caused by the addition of the metal ions are larger than the red shift induced by the resonance coupling and that the extinction peak becomes more asymmetric with

(49) Rao, T. P.; Reddy, M. L. P.; Pillai, A. R. *Talanta* **1998**, *46*, 765–813.
(50) Raj, M. M.; Dharmaraja, A.; Kavitha, S. J.; Panchanatheswaran, K.; Lynch, D. E. *Inorg. Chem. Acta* **2007**, *360*, 1799–1808.

increasing metal ion concentrations (compare Figure 7a with Figure S6 in the Supporting Information). These results can be hypothetically ascribed to the change in the electrical double layer structure and thus the local refractive index at the solid−liquid interface around the hybrid nanostructures caused by high concentrations of the metal ions. This change acts together with the resonance decoupling to result in the observed extinction spectral variations.

Conclusion

We have constructed Au nanocrystal−organic dye hybrid nanostructures and studied how the resonance coupling behavior depends on the plasmonic properties of the Au nanocrystals, the molecular properties of the dyes, the solution pH, and metal ions. The resonance coupling strength is found to approximately increase as the molecular volume-normalized absorptivity is increased. It is mainly determined by the plasmon resonance energy, instead of the Au nanocrystal shape and size. The resonance coupling can be weakened or even reversibly turned on and off by adding metal ions or adjusting the solution pH, respectively. These findings will be highly useful for designing and fabricating ultrasensitive, resonance coupling-based sensing devices and for plasmon-enhanced spectroscopy.

Acknowledgment. This work was supported by National Natural Science Foundation of China (Project Code: 20828001), CUHK Research Excellence Award 2008−2009 (Project Code: 4411435), RGC Research Grant Direct Allocation (Project Code: 2060358), and DuPont Young Professor Grant (H.K.W., 2007−2009). We thank Alexander Wei from the Department of Chemistry of Purdue University and Luis M. Liz-Marzán from Departmento de Química Física and Unidad Asociada CISC of Universidade de Vigo for helpful discussions.

Supporting Information Available: Curve fitting, the extinction spectra of the PSS-coated Au nanocrystals in the presence of the different dye molecules at varying concentrations, the molecular structures and solvent-accessible surfaces of the dye molecules, the extinction spectra of the differently shaped Au nanocrystals and the corresponding nanorod−HITC hybrid samples, the absorption spectra of HITC at different pHs, the effects of the metal ions on the resonance coupling between the Au nanorods and dye molecules, and the absorption spectra of the dye molecules and the extinction spectra of the Au nanorods acquired in the presence of the metal ions at varying concentrations. This material is available free of charge via the Internet at http://pubs.acs.org.

JA910239B